



Integration of a DC Transformer, Four-Leg Inverter, and Flexible Grid Input into the Consolidated Utility Base Electrical (CUBE) System

Mariko Shirazi
National Renewable Energy Laboratory

Christopher Niebylski and John Deplitch
Wyle Laboratories

Produced under direction of Wyle Laboratories by the National Renewable Energy Laboratory (NREL) under Work for Others Agreement number FIA-15-1811 and Task No. WWGZ.1000.

**NREL is a national laboratory of the U.S. Department of Energy
Office of Energy Efficiency & Renewable Energy
Operated by the Alliance for Sustainable Energy, LLC**

This report is available at no cost from the National Renewable Energy Laboratory (NREL) at www.nrel.gov/publications.

Strategic Partnership Project Report
NREL/TP-5D00-66612
June 2016

Contract No. DE-AC36-08GO28308



Integration of a DC Transformer, Four-Leg Inverter, and Flexible Grid Input into the Consolidated Utility Base Electrical (CUBE) System

Mariko Shirazi
National Renewable Energy Laboratory

Christopher Niebylski and John Deplitch
Wyle Laboratories

Prepared under Task No. WWGZ.1000

**NREL is a national laboratory of the U.S. Department of Energy
Office of Energy Efficiency & Renewable Energy
Operated by the Alliance for Sustainable Energy, LLC**

This report is available at no cost from the National Renewable Energy Laboratory (NREL) at www.nrel.gov/publications.

NOTICE

This manuscript has been authored by employees of the Alliance for Sustainable Energy, LLC (“Alliance”) under Contract No. DE-AC36-08GO28308 with the U.S. Department of Energy (“DOE”).

This report was prepared as an account of work sponsored by an agency of the United States government. Neither the United States government nor any agency thereof, nor any of their employees, makes any warranty, express or implied, or assumes any legal liability or responsibility for the accuracy, completeness, or usefulness of any information, apparatus, product, or process disclosed, or represents that its use would not infringe privately owned rights. Reference herein to any specific commercial product, process, or service by trade name, trademark, manufacturer, or otherwise does not necessarily constitute or imply its endorsement, recommendation, or favoring by the United States government or any agency thereof. The views and opinions of authors expressed herein do not necessarily state or reflect those of the United States government or any agency thereof.

Acknowledgements

Over the past seven years, the CUBE has grown from an idea to a functional prototype. The project has been funded by the U.S. Department of Defense. First and foremost, the authors would like to thank key individuals from the sponsoring agencies: Mr. Christopher Bolton from the Army Expeditionary Energy and Sustainment Systems (E2S2), and COL (R) Steven A. Sliwa, LTC Jennifer R. Zais, and Mr. Andrew E. Yuliano from the Army Rapid Equipping Force (REF). Many others have contributed to build the CUBE from a pile of parts. Many of these people have been recognized in an earlier report documenting the performance of CUBE-V1. However, additional acknowledgement and gratitude is due those who supported the CUBE-V2 work. In particular, the authors would like to thank the following: Bob Hansen, who originally built the entire CUBE-V1 and also disassembled and rebuilt it as CUBE-V2—the CUBE would not exist without him; Mark Murphy, who without knowing anything about the CUBE, stepped in to complete all the CUBE-V2 power and signal wiring; Mike Dooraghi, who took on the tedious task of double-checking every wiring connection; and members of the Energy Systems Integration Facility (ESIF) Area Work Supervisors and electrician staff—Kyle Tangler, Darin Smith, Sergio Yebra, Don Finley, and Tom Bethel, who were always available to assist with hardware modifications, electrical installation, and tactical quiet generator (TQG) fuel modifications. Finally, CUBE acknowledgements would never be complete without including the CUBE visionary Bill Kramer and CUBE co-designer Greg Martin.

List of Acronyms

3D-SVM	three-dimensional space-vector modulation
AC	alternating current
ACV	Main AC bus voltage regulation
BCD	battery charge/discharge
BW	band width
COP	Command Outpost
cRIO	CompactRIO
CUBE	Consolidated Utility Base Energy
DAB	dual active bridge
DAQ	data acquisition
DC	direct current
DCX	DC transformer
E2S2	Expeditionary Energy and Sustainment Systems
EMI	Electromagnetic Interference
ESIF	Energy Systems Integration Facility
FLI	four-leg inverter
FOB	Forward Operating Base
FPGA	field-programmable gate array
GCI	grid-connected inverter
HFX	high-frequency transformer
IGBT	insulated-gate bipolar transistor
MPPT	máximum-power-point tracking
NREL	National Renewable Energy Laboratory
PID	proportional-integral-derivative
PLL	phase-locked loop
PV	photovoltaic
PVC	photovoltaic converter
PWM	pulse-width modulation
REDB	Research Electrical Distribution Bus
REF	Rapid Equipping Force
RLC	resistive, inductive, and capacitive
RMS	root mean square
SVM	space-vector modulation
TQG	Tactical Quiet Generator
ZVS	zero-voltage switching

Table of Contents

Acknowledgements	iii
List of Acronyms	iv
Table of Contents	v
List of Figures	vi
List of Tables	vii
Executive Summary	1
1. Introduction	2
2. CUBE-V2 Architecture	4
2.1. DC Transformer.....	6
2.2. Four-Leg Inverter	7
2.3. Grid-Connected Inverter.....	8
2.4. Battery Charger/Discharger.....	9
2.5. PV MPPT Converters (PVCs).....	9
3. CUBE-V2 Operating Modes	10
4. Experimental Equipment	13
4.1. CUBE	13
4.2. Diesel Generators	13
4.3. Battery Simulator.....	14
4.4. Grid Simulator	14
4.5. Load Bank	14
4.6. CUBE Liquid-Cooling System 24-V Power Supply	15
4.7. Data Acquisition (DAQ) System.....	15
5. Experimental Results	18
5.1. Battery-Only Results	18
Observations during Battery-Only Operation	21
5.2. GCI-Only Results	22
Observations during Grid-Only Operation.....	25
5.3. Diesel + Battery + Grid Results.....	25
Observations during Operation with Diesels, Battery, and Grid.....	29
5.4. Leakage Current	30
5.5. Efficiency	31
6. Conclusions and Future Work	32
7. References	33

List of Figures

Figure 1. CUBE Version 1 (CUBE-V1) block diagram.	3
Figure 2. CUBE Version 2 (CUBE-V2) block diagram.	3
Figure 3. CUBE-V2 three-line diagram.	5
Figure 4. Prototype HFX and resonant inductor. <i>Photo by Mariko Shirazi, NREL</i>	7
Figure 5. Consolidated Utility Base Energy (CUBE). <i>Photo by Dennis Schroeder, NREL</i>	13
Figure 6. Tactical Quiet Generator (TQG) sets. <i>Photo by Dennis Schroeder, NREL</i>	14
Figure 7. CUBE in Battery-Only mode, FLI waveforms during (a) +30-kW and (b) -30-kW balanced load steps.	19
Figure 8. CUBE in Battery-Only mode, HFX waveforms at (a) no load and (b) 30-kW balanced load. ...	19
Figure 9. CUBE in Battery-Only mode and high proportional gain for 0-component of FLI voltage control PID feedback loop, FLI voltage and current waveforms at balanced 21-kW load (a,b) and unbalanced (c,d) load with $PhA = 12$ kW, $PhB = 6$ kW, and $PhC = 3$ kW.	20
Figure 10. CUBE in Battery-Only mode and high proportional gain for 0-component of FLI voltage control PID feedback loop, DAB waveforms at (a) 21-kW balanced load and (b) unbalanced load of $PhA = 12$ kW, $PhB = 6$ kW, and $PhC = 3$ kW.	21
Figure 11. CUBE in Grid-Only mode, FLI waveforms during (a) +15-kW and (b) -15-kW balanced load steps.	22
Figure 12. CUBE in Grid-Only mode, DAB waveforms at (a) no load and (b) 15-kW balanced load.	23
Figure 13. CUBE in Grid-Only mode and high proportional gain for 0-component of FLI voltage control PID feedback loop, FLI voltage and current waveforms at balanced 15-kW load (a,b) and unbalanced load (c,d) with $PhA = 8$ kW, $PhB = 4$ kW, and $PhC = 2$ kW.	24
Figure 14. CUBE in Grid-Only mode and high proportional gain for 0-component of FLI voltage control PID feedback loop, DAB waveforms at (a) 15-kW balanced load and (b) unbalanced load of $PhA = 8$ kW, $PhB = 4$ kW, and $PhC = 2$ kW.	25
Figure 15. CUBE in Diesel + Battery + Grid mode and 25-kW load applied, FLI and BCD waveforms during (a) 0 to +67 A and (b) +67 to 0 A steps in battery reference current, with grid reference current = 0.	26
Figure 16. CUBE in Diesel + Battery + Grid mode and no load, FLI and BCD waveforms during (a) 0 to -67 A and (b) -67 to 0 A steps in battery reference current, with grid reference current = 0.	26
Figure 17. CUBE in Diesel + Battery + Grid mode and no load, FLI and BCD waveforms during (a) -67 A steady state and (b) 0 to -50 A steps in battery reference current, with grid reference current = 0.	27
Figure 18. CUBE in Diesel + Battery + Grid mode and 25-kW load applied, FLI and GCI waveforms during (a) 0 to -50 A and (b) -50 to 0 A steps in grid reference current, with battery reference current = 0.	27
Figure 19. CUBE in Diesel + Battery + Grid mode and no load, FLI and GCI waveforms during (a) 0 to +50 A and (b) +50 to 0 A steps in grid reference current.	28
Figure 20. CUBE in Diesel + Battery + Grid mode, DAB waveforms at (a) 25-kW load and battery reference current of +67 A and (b) no load and battery reference current of -67 A, with grid reference current = 0.	28
Figure 21. CUBE in Diesel + Battery + Grid mode, 10 μ s/div zooms of DAB waveforms at (a) 25-kW load and battery reference current of +67 A and (b) no load and battery reference current of -67 A, with grid reference current = 0.	29

Figure 22. Leakage current and common-mode voltage on the secondary-side DC bus during operation (a) in Battery-Only mode at 30 kW, and (b) Diesel + Battery + Grid mode, 25-kW load, battery reference current = +67 A, and (c) Diesel + Battery + Grid mode, 5-kW load, battery reference current = -67 A.... 31

List of Tables

Table 1. CUBE-V2 System Operating Modes	11
Table 2. DAQ Signals, Probes, Input Modules, and Bandwidth (BW) Limits	16

Executive Summary

This report describes design improvements and test validation of these improvements to the National Renewable Energy Laboratory's (NREL's) Consolidated Utility Base Energy (CUBE) system. The first version of the CUBE, "CUBE-V1," was designed, built, and tested between 2009 and 2014 and is documented in a previous NREL Technical Report, NREL/TP-5B00-52768, "Consolidated Utility Base Energy (CUBE) Performance Test Report." Similar to CUBE-V1, the new "CUBE-V2" design provides power conversion, distribution, and protection necessary to integrate photovoltaic arrays, a battery bank, and diesel generators. In addition, the CUBE-V2 design includes the following improvements:

- (1) *Decrease in the size and weight of the design* by replacing the line-frequency transformer with a DC-DC transformer (DCX), consisting of a smaller high-frequency rated transformer, additional magnetics, and power-electronic switches to realize a smaller and lighter CUBE;
- (2) *Ability to balance voltage under unbalanced load conditions* through the addition of a fourth leg to the CUBE inverter;
- (3) *Provision for the connection to host-nation grids of varying voltage, frequency, and power quality* through the addition of a flexible grid port.

To validate the design modifications, experimental waveforms were captured during operational testing of the CUBE-V2 to verify new functionalities as well as observe output power quality and dynamic response. As shown in this report, the experimental results indicate that the intended design targets were achieved.

Specifically, combined operation of a dual-active bridge (DAB) and a four-leg inverter (FLI) can provide the galvanic isolation and neutral connection traditionally supplied by a three-leg inverter and line-frequency transformer with significantly reduced weight and volume (a 55% reduction in volume and a 70% reduction in weight relative to the line-frequency transformer). Furthermore, the DAB-FLI solution can provide voltage-balancing functionality that the traditional configuration could not. Provision for connection to a host utility through the improved design was also validated.

The advantages demonstrated by the CUBE-V2 design are significant improvements upon the CUBE-V1 design, making it lighter, smaller, and more flexible for field operations. These improvements should yield logistical and operational benefits to mobile electric power systems such as those employed to provide power to Forward Operating Bases and Command Outposts.

1. Introduction

The Consolidated Utility Base Energy (CUBE) system is an integrated power electronic platform for a 60-kW photovoltaic (PV)-battery-diesel hybrid power system developed for the U.S. Army Rapid Equipping Force (REF) and the Expeditionary Energy and Sustainment Systems (E2S2) to reduce use of diesel fuel at Forward Operating Bases (FOBs). The CUBE is based on modular power-electronic building blocks and includes power distribution and protection components, an isolation transformer, magnetics and other filter components, a liquid-cooling system, a control platform based on field-programmable gate array (FPGA) and real-time controllers, and a touchscreen user interface. The original version of the CUBE—herein referred to as “CUBE-V1,” shown in Figure 1—was able to integrate four 5- to 10-kW PV arrays, one 30-kW battery pack, and two 30-kW diesel generator sets to power a 60-kW peak load. This version of the CUBE included a line-frequency transformer to provide galvanic isolation between the alternating current (AC) and direct current (DC) buses and to provide a neutral connection for single-phase loads.

The new version of the CUBE—herein referred to as “CUBE-V2”—includes the following improvements:

- (1) *Decrease in the size and weight of the design* by replacing the line-frequency transformer with a DC-DC transformer (DCX), consisting of a smaller high-frequency rated transformer, additional magnetics, and power-electronic switches to realize a smaller and lighter CUBE;
- (2) *Ability to balance voltage under unbalanced load conditions* through the addition of a fourth leg to the CUBE inverter;
- (3) *Provision for the connection to host-nation grids of varying voltage, frequency, and power quality* through the addition of a flexible grid port.

These modifications required incorporating new power electronics and reconfiguring the existing power electronics such that, as shown in Figure 2, CUBE-V2 is able to integrate three 5- to 10-kW PV arrays, one 30-kW battery pack, one 50-kW grid connection, and two 30-kW diesel generator sets. The loss of one of the PV inputs was necessary to accommodate the new functionalities.

The remainder of this report describes the V2 architecture and presents experimental waveforms showing operation of the new components in CUBE-V2. The report is organized as follows:

- Section 2: Overview of CUBE-V2 power and control architectures
- Section 3: Overview of CUBE-V2 operating modes
- Section 4: Description of experimental equipment
- Section 5: Experimental results
- Section 6: Conclusions and future work.

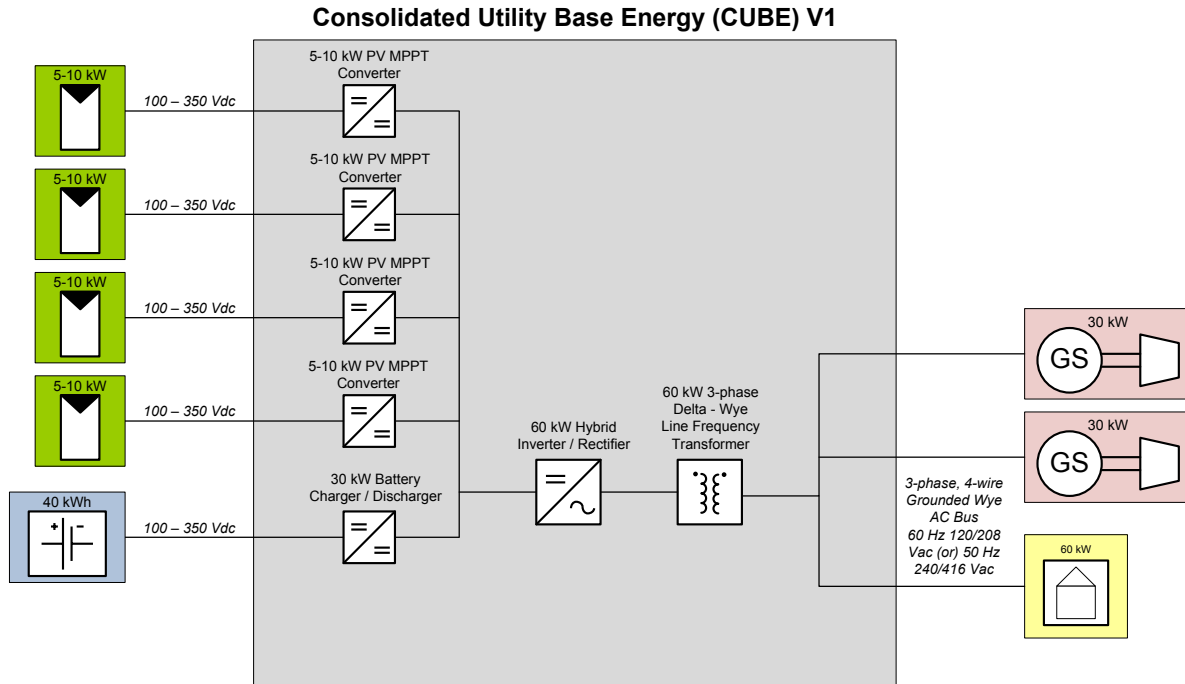


Figure 1. CUBE Version 1 (CUBE-V1) block diagram.

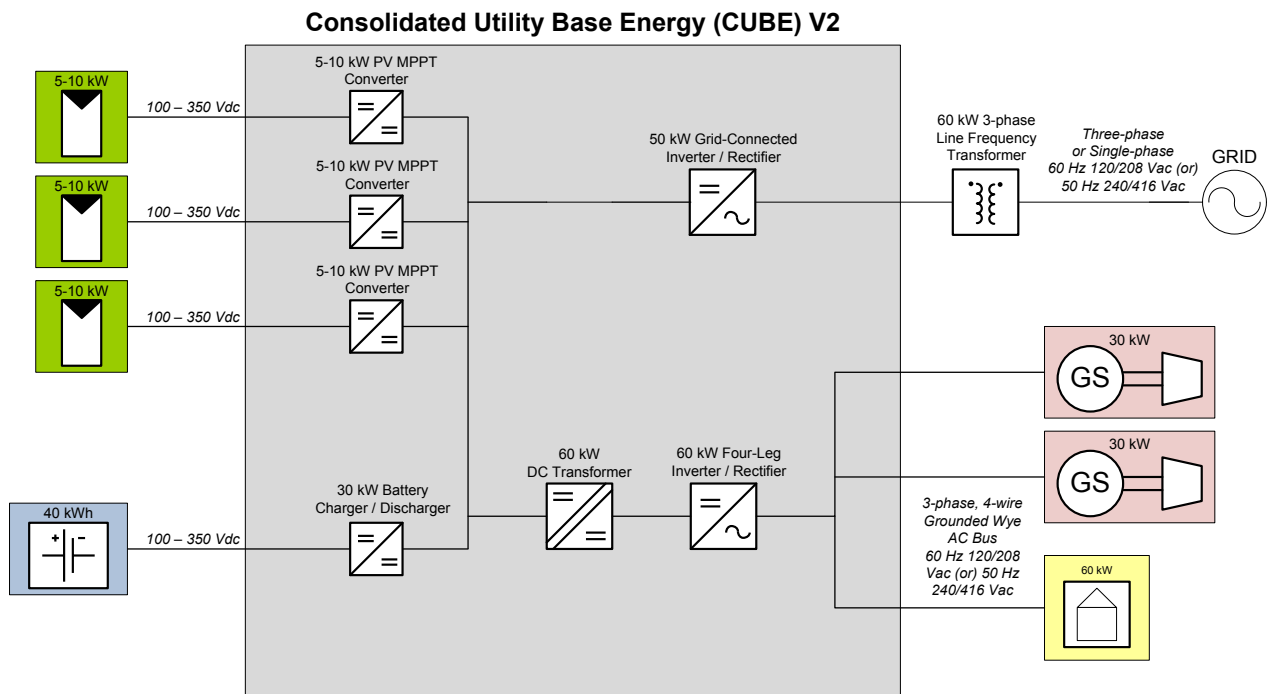


Figure 2. CUBE Version 2 (CUBE-V2) block diagram.

2. CUBE-V2 Architecture

The power electronic switches for both CUBE-V1 and CUBE-V2 are implemented using Semikron SKAI modules. These are liquid-cooled modules that include insulated-gate bipolar transistor (IGBT) power semiconductors, DC link capacitors, gate drivers with low-level protection, and sensors for voltage, current, and temperature. NREL specified the power electronic topologies and filter components for each converter. Common converters to both CUBE versions include PV converters (PVCs) to provide maximum-power-point tracking (MPPT) for the PV inputs, a battery charge/discharge (BCD) converter to interface with the battery, and a bi-directional inverter capable of operating either as the grid-forming unit or in parallel with other voltage sources such as diesel generators.

In the case of CUBE-V2, the latter functionality is provided by a four-leg inverter (FLI), which includes a fourth switched leg to serve single-phase loads and to provide voltage balancing in the presence of unbalanced loads. In addition, CUBE-V2 includes another bi-directional inverter, the grid-connected inverter (GCI), to allow connection to host-nation grids or other diesel generators of varying voltage and/or frequency. Finally, CUBE-V2 includes a DC transformer (DCX) to provide galvanic isolation between the main AC bus, which includes the base loads and diesel generators, from alternate power sources such as PV, battery, and a host utility connection. Each of the converter topologies is depicted in the blue-bordered boxes of the CUBE-V2 three-line diagram in Figure 3. In this diagram, the primary-side DC bus is defined as the DC bus to which the battery, PV arrays, and grid are connected, whereas the secondary-side DC bus is as the DC bus to which the main AC bus, including diesel generators and loads, is connected.

For each converter, modulation and feedback control algorithms were developed to provide the required converter functionalities. The control platform is based on National Instruments' CompactRIO (cRIO) modules, each of which includes an FPGA backplane and a real-time processor. All local control-level algorithms were implemented in LabVIEW FPGA and include the pulse-width modulation (PWM) or space-vector modulation (SVM) algorithms necessary to generate the gate drive commands for the power electronics and the proportional-integral-derivative (PID) algorithms necessary to operate the converter in various feedback control modes (such as voltage control, current control, or MPPT).

Each of the V2 converters is described in more detail in the following sections.

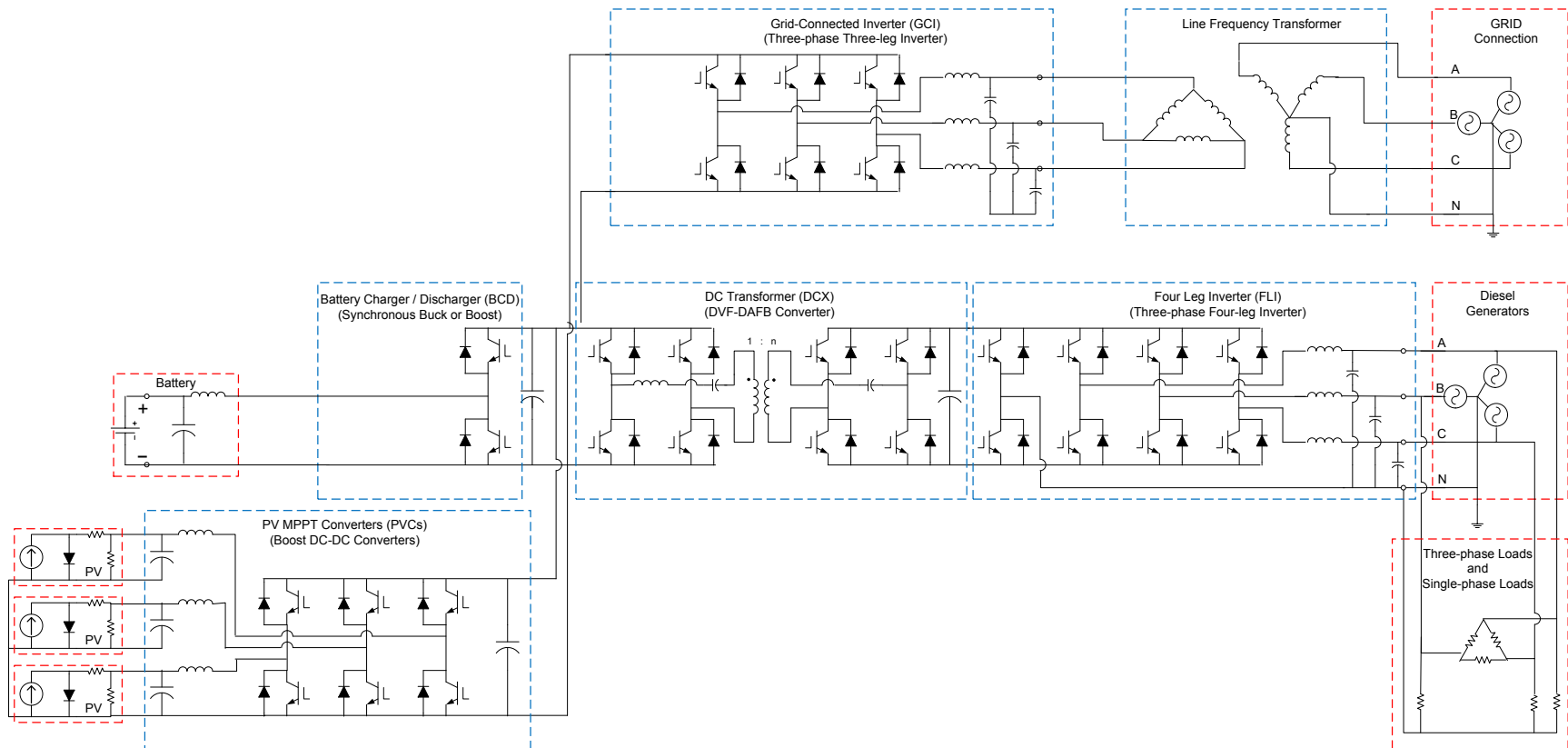


Figure 3. CUBE-V2 three-line diagram.

2.1. DC Transformer

CUBE-V1 included a 75-kVA (60 kW at 0.8 power factor) three-phase delta:wyne line-frequency (50 or 60 Hz) transformer to provide galvanic isolation between the main AC bus and the DC sources. Although robust, the transformer is bulky (8.1 ft³) and heavy (575 lbs.). In CUBE-V2, the isolation is instead provided by the 60-kW DCX. The DCX is an isolated bi-directional DC-DC converter designed to operate at a fixed conversion ratio, M , defined by $M = V_{out}/nV_{in}$, where V_{out} is the primary-side DC bus voltage, V_{in} is the secondary-side DC bus voltage, and n is the transformer turns ratio.

There are multiple isolated DC-DC converter topologies that could have been used to implement the DCX. However, the dual active bridge (DAB) topology was chosen due to the simplicity and symmetry of the topology, as well as the opportunities to employ symmetric soft-switching control algorithms. The topology was first introduced in Ref. [1] and patented in Ref. [2] (the patent expired in 2008), and it may employ either resonant-transition or full-resonant network structures and control methods [3–7]. To maintain high efficiency, it is desirable to operate the DAB with zero-voltage switching (ZVS) and to minimize the high-frequency transformer current. With full-resonant topologies, it is difficult to achieve high efficiencies over a wide range of output power levels.

For resonant-transition topologies, there are multiple modulation strategies from which to select [7–11]. The simplest is to drive both primary- and secondary-side H bridges with 50% duty cycles to generate square waves and then to phase-shift one square wave with respect to the other to control power flow. The phase-shift modulation approach has disadvantages when operating over wide conversion ratios—notably, reduced range of power levels over which ZVS is maintained and increased transformer current. However, the approach is able to achieve high efficiency and low transformer currents over the entire power range when operating at a conversion ratio of unity [7–11], i.e., as a 1:1 DCX.

As shown in Figure 3, the CUBE-V2 DCX is based on a dual-voltage-fed DAB topology, including a high-frequency (10-kHz) transformer, a resonant inductor, primary- and secondary-side H bridges, and DC-blocking capacitors. For this work, the DAB was implemented in hardware using a prototype air-cooled, high-frequency transformer (HFX) and resonant inductor, two out of the three legs from two different SKAIs for the H bridges, and film capacitors to prevent transformer saturation. The 10-kHz rated transformer and resonant inductor were built by CTM Magnetics according to NREL-provided specifications. The transformer turns ratio n can be configured to be unity for CUBE operation when both the main AC bus and the grid connection have similar voltages (e.g., either both 120/208 and both 240/416), or $1/2$ when the main AC bus is at the standard 120/208 and the grid connection is at 240/416.

The prototype HFX and resonant inductor are shown in Figure 4. The combined volume and weight of the prototype magnetics, two SKAI modules, and the two DC blocking capacitors is 3.6 ft³ and 174 lbs., which is a 55% reduction in volume and a 70% reduction in weight relative to the line-frequency transformer. Custom, non-modular design of a DAB could further increase the volume and weight savings.



Figure 4. Prototype HFX and resonant inductor. Photo by Mariko Shirazi, NREL

The CUBE-V2 DAB is controlled with phase-shift modulation. A PID feedback loop generates the phase-shift command to regulate a constant conversion ratio of unity, regardless of what the actual voltage happens to be. The CUBE includes mode-handling algorithms to ensure that only one of the primary or secondary DC buses is being regulated at any given time. The DAB then transfers power as necessary to regulate the other bus at the same voltage.

2.2. Four-Leg Inverter

In addition to providing galvanic isolation, the CUBE-V1 delta:wyne line-frequency transformer also derived the neutral necessary to serve single-phase loads. Replacement of this line-frequency transformer with a DCX required that the CUBE inverter must now generate a neutral natively in order to continue to serve single-phase loads. Three topologies accomplish this: split DC bus, three single-phase H bridges, and a four-leg inverter. In a *split DC bus inverter*, the DC bus capacitance is split in half and the neutral is connected to the center point. However, this topology requires large capacitors to supply zero sequence current and consideration of voltage imbalance across the capacitors. In the *three single-phase H bridge* topology, three separate single-phase H bridges are used to generate each phase with the neutrals all tied together. This topology typically requires generation of three isolated DC buses to feed each half-bridge. In a *four-leg inverter*, the neutral is instead connected to the switch-node of a fourth inverter half-bridge. Compared to the *split DC bus inverter*, this topology allows for the use of smaller DC bus capacitors and does not require voltage balancing across the capacitors; compared to the *three single-phase H bridge*, this topology does not require three isolated DC buses and in addition requires two fewer switches. The only disadvantage of the *four-leg inverter* topology is the relative control complexity; however, this was a surmountable challenge given the powerful FPGA-based control platform of the CUBE. Therefore, the *four-leg inverter* topology was chosen for this design.

The CUBE-V2 FLI is controlled with three-dimensional SVM (3D-SVM) [12,13] in which the space vectors are located in three-dimensional prisms versus two-dimensional sectors. Three PID feedback loops executing in the direct-quadrature-zero (dq0) synchronous reference frame regulate the abc voltages or currents depending on the FLI operating mode. The loop dq0 outputs are transformed via the Park Transform to generate the $\alpha\beta\gamma$ command for the 3D-SVM.

The FLI can operate as the grid-forming unit or in parallel with another voltage source such as the diesel generators. When operating as the grid-forming unit, the FLI is in voltage control mode, regulating the abc output voltages to a fixed q-axis reference, with both d-axis and 0-axis references at zero. When operating in parallel with the diesel generators, the FLI is in current control mode, regulating the abc current. In this mode, an outer DC bus voltage loop generates the q-axis current command (corresponding to real power), the d-axis current command (corresponding to reactive power)¹ is externally provided, and the 0-axis current command is set to zero. Finally, the FLI can also synchronize to the external voltage source. During synchronization, the FLI is in voltage control mode, regulating the abc voltages to match the magnitude, frequency, and phase angle of the external source. The synchronizing mode allows a seamless transition from operation of the FLI as the grid-forming unit to operation in parallel with the diesel generators or another voltage source.

2.3. Grid-Connected Inverter

Rather than connecting directly to the main AC bus, the CUBE grid input is rectified via the GCI onto the primary-side DC bus. This allows connection to grids of varying voltage and frequency and, importantly, with potentially poor power quality.

Like the FLI, the GCI is a bi-directional inverter; however, it only has three legs and is controlled with standard two-dimensional SVM. In addition, because there are no loads connected directly to the GCI port, there is no need for the GCI to operate in voltage control mode or to be able to synchronize to the grid. Instead, the contactor can be closed when the GCI is off and then the GCI can go directly into current control mode. This is typical of most grid-connected inverters.

Because the DCX isolates the primary- and secondary-side DC buses, it is possible to connect the CUBE GCI directly to a ground-referenced grid, foregoing the external line-frequency transformer shown in Figure 3. However, this would introduce a high-frequency common-mode voltage component onto the battery and PV sources. Theoretically, this should not be a problem if the battery and PV sources are floating. However, in practice, most floating battery packs greater than 100 V include isolation-monitoring devices that will trip the battery off-line upon identifying a ground reference. The programmable DC power supply used to emulate the battery for this testing includes this type of ground-fault protection; thus, the external line-frequency transformer is necessary.²

¹ The convention in this work is based on sine vs. cosine waveforms – i.e., the instantaneous angle generated by the PLL is zero at the rising edge zero crossing of Phase A. This convention maps the negative q-axis current to real power and the negative d-axis current to reactive power.

² Direct connection of a ground-referenced AC bus to either the CUBE GCI port or the FLI port also introduces a path for high-frequency common-mode current through the SKAI Y-capacitors back to the respective DC bus. This is discussed in further detail in the experimental results of Section 5.

2.4. Battery Charger/Discharger

The BCD is a half-bridge that operates as a synchronous boost converter when discharging the battery and a synchronous buck converter when charging the battery. The BCD is controlled with standard PWM of the switches and feedback loops, which allows current control, DC bus voltage regulation, or regulation of the battery voltage (for float charging).

2.5. PV MPPT Converters (PVCs)

The PVCs are simple boost converters controlled with standard PWM of the switch and an inner feedback loop regulating PV voltage. In most cases, the voltage reference is provided by an outer perturb-and-observe MPPT algorithm. However, the PVCs also include an outer DC bus voltage regulation loop that can be used to pre-charge the DC bus during start-up of the CUBE.

3. CUBE-V2 Operating Modes

The possible set of CUBE-V2 system operating modes are listed in Table 1 using the following acronyms:

- ACV: Main AC Bus Voltage Regulation
- DCV: DC Bus Voltage Regulation
- MREG: Conversion Ratio Regulation (regulating to $M = 1$)
- CC: Current Control
- BV: Battery Voltage Regulation
- MPPT: Maximum-Power-Point Tracking

The primary goal of the control system is to regulate the main AC bus and the DC buses. The CUBE-V2 system operating modes can be classified according to which component regulates each bus. Table 1 is shaded to reflect this categorization.

- Pink shading: FLI regulates main AC bus, BCD regulates DC bus
- Blue shading: FLI regulates main AC bus, GCI regulates DC bus
- Yellow shading: TQG regulates main AC bus, FLI regulates DC bus
- Green shading: FLI regulates main AC bus, PVC regulates DC bus
- Orange shading: TQG regulates main AC bus, all power electronics OFF
- Gray shading: All components OFF

Table 1. CUBE-V2 System Operating Modes

Mode \ Component	TQG	FLI	PVC	BCD	GCI	DAB
OFF	OFF	OFF	OFF	OFF	OFF	OFF
Diesel Only	ACV	OFF	OFF	OFF	OFF	OFF
Diesel + PV MPPT	ACV	DCV	MPPT	OFF	OFF	MREG
PV Only	OFF	ACV	DCV	OFF	OFF	MREG
Diesel + Battery Current	ACV	DCV	OFF	CC	OFF	MREG
Diesel + Battery Voltage	ACV	DCV	OFF	BV	OFF	MREG
Battery Only	OFF	ACV	OFF	DCV	OFF	MREG
Diesel + PV MPPT + Battery Current	ACV	DCV	MPPT	CC	OFF	MREG
Diesel + PV MPPT + Battery Voltage	ACV	DCV	MPPT	BV	OFF	MREG
PV + Battery	OFF	ACV	MPPT	DCV	OFF	MREG
Grid Only	OFF	ACV	OFF	OFF	DCV	MREG
Diesel + Grid	ACV	DCV	OFF	OFF	CC	MREG
Diesel + PV MPPT + Grid	ACV	DCV	MPPT	OFF	CC	MREG
PV + Grid	OFF	ACV	MPPT	OFF	DCV	MREG
Diesel + Battery Current + Grid	ACV	DCV	OFF	CC	CC	MREG
Diesel + Battery Voltage + Grid	ACV	DCV	OFF	BV	CC	MREG
Battery + Grid	OFF	ACV	OFF	DCV	CC	MREG
Diesel + PV MPPT + Battery Current + Grid	ACV	DCV	MPPT	CC	CC	MREG
Diesel + PV MPPT + Battery Voltage + Grid	ACV	DCV	MPPT	BV	CC	MREG
PV + Battery + Grid	OFF	ACV	MPPT	DCV	CC	MREG

The following are comments regarding the CUBE-V2 operating modes:

- Components operating in DCV control actually regulate the DC bus voltage to which they are attached. That is, the BCD and GCI regulate the primary-side DC bus, whereas the FLI regulates the secondary-side DC bus. The DAB transfers power as necessary to match the two DC bus voltages.
- Not all of the possible control modes for a particular component show up in the table of system operating modes. This is because these component control modes are only used when the CUBE is transitioning from one system operating mode to another. For example, the FLI can operate in a synchronizing control mode where it synchronizes its voltage output to match that of the diesel generators.
- During operation of the FLI as the grid-forming unit (AC Voltage Control - ACV) and when both the BCD and the GCI are on line, it is possible to choose either the BCD or the GCI to regulate DC bus voltage. In this case, the BCD is chosen to regulate the DC bus in order to maximize reliability in the presence of uncertain grid conditions.
- During operation of the FLI in parallel with the diesel generators, and when the BCD and/or GCI is on line, it is possible to choose the FLI, BCD, or GCI to regulate the DC bus. In this case, the FLI is chosen to regulate the DC bus in order to most efficiently

deliver any PV power to the main AC bus and not into the battery or onto the grid. (Battery charging is allowed to occur if there is excess PV.)

- The PV-Only operating mode is included for completeness; however, the CUBE dispatch strategy will never enter this operating mode. Instead, the dispatch strategy requires that any portion of the load being met by PV must be 100% matched by reserve diesel, battery, or grid capacity. This prevents loss of power in the case that PV output from all producing panels suddenly plummets (e.g., due to a passing cloud, blinding sandstorm, or low-flying C-130).

4. Experimental Equipment

During the experimental validation stage of this project, the following equipment was used.

4.1. CUBE

The CUBE is shown in Figure 5.

- Manufacturer: NREL
- Model No: Prototype
- Power: 60 kW
- Main AC Bus Voltage: 120/208 Vac or 240/416 Vac
- Main AC Bus Frequency: 60 Hz or 50 Hz

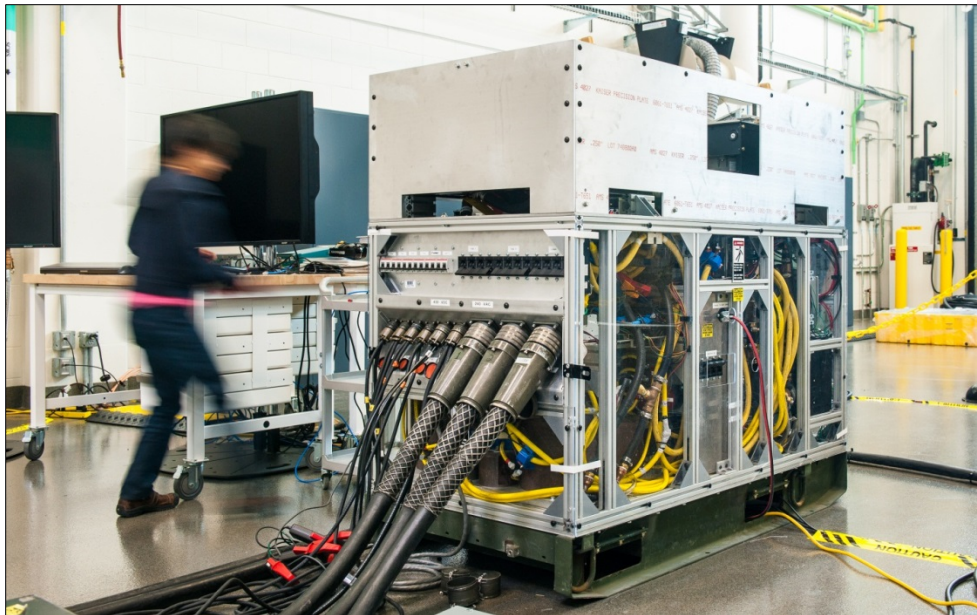


Figure 5. Consolidated Utility Base Energy (CUBE)³. Photo by Dennis Schroeder, NREL

4.2. Diesel Generators

The two 30-kW tactical quiet generators (TQGs) are shown in Figure 6.

- Manufacturer: L-3 Communications Westwood Corporation
- Model No: MEP-805B
- Power: 30 kW
- Voltage: 120/208 Vac or 240/416 Vac
- Frequency: 60 Hz or 50 Hz

³ This is actually a photo of the CUBE-V1, but CUBE-V2 looks very similar from the exterior.

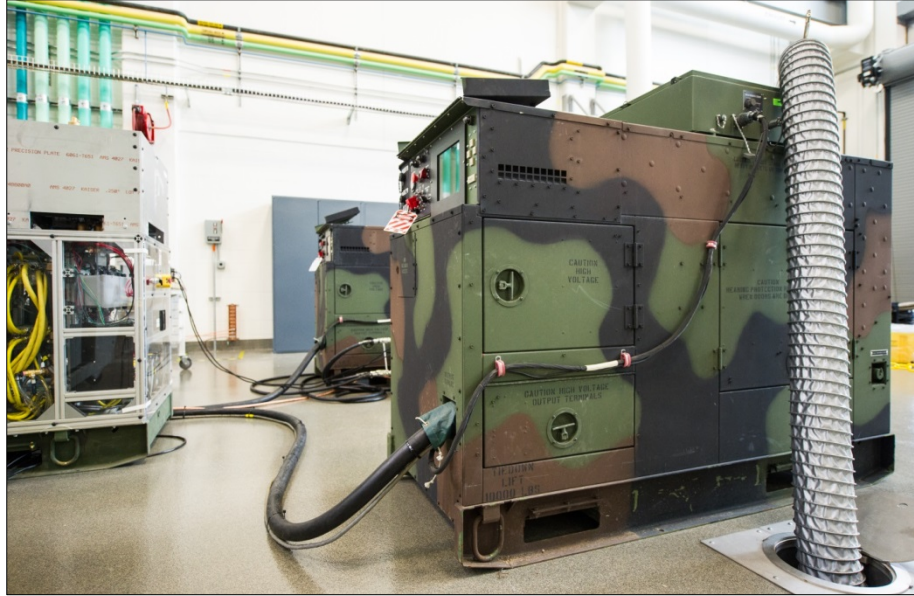


Figure 6. Tactical Quiet Generator (TQG) sets. Photo by Dennis Schroeder, NREL.

4.3. Battery Simulator

A bi-directional programmable DC power supply was used to emulate the battery input to the CUBE.

- Manufacturer: AeroVironment
- Model No: AV-900
- Voltage: 900 Vdc
- Current: 500 Adc (per channel)

4.4. Grid Simulator

A three-phase bi-directional programmable AC power supply was used to emulate the grid connection to the CUBE.

- Manufacturer: Ametek
- Model No: MX45
- Voltage: 690 Vac
- Current: 50 Aac

4.5. Load Bank

The CUBE load output was connected to an outdoor load bank via the Energy Systems Integration Facility (ESIF) Research Electrical Distribution Bus (REDB). The load bank is a three-phase resistive, inductive, and capacitive (RLC) load bank rated at 250 kW / 250 kVAR inductive / 250 kVAR capacitive at 277/480 V. The ratings at 120/208 V are 46 kW / 46 kVAR inductive / 46 kVAR capacitive. The inductive and capacitive capability of the load bank was not used for this testing.

- Manufacturer: LoadTec
- Model No: OSW4c-0390.7-600v34-456D-50w
- Power: 46 kW / 46 kVAR inductive / 46 kVAR capacitive at 120/208 Vac
- Single-Phase Load Step Resolution: 10 W at 120 Vac.

4.6. CUBE Liquid-Cooling System 24-V Power Supply

An external 24-V power supply was required to power the CUBE liquid-cooling system. Future modifications to the CUBE will allow self-generation of the 24-V power for the liquid-cooling system.

- Manufacturer: Chroma
- Model No: 62024P-100-50
- Voltage: 100 Vdc
- Current: 50 Adc

4.7. Data Acquisition (DAQ) System

A Yokogawa DL850 “ScopeCorder” was used to measure and record data.

- Manufacturer: Yokogawa
- Model No: DL850-D-HE/M1HD1/G2/G3/P4

The DL850 frame accepts up to eight input modules, with two channels per module. The following Yokogawa input modules were used:

- 701210 High-Speed 100 MS/s 12-bit Isolated Analog Input Module, Bandwidth: 20 MHz
- 701260 High-Voltage 100 kS/s 16-bit Isolated Analog Input Modules with RMS, Bandwidth: 40 kHz

The following voltage and current probes were used:

- Yokogawa 700929 10: 1 Passive Voltage Probe, Bandwidth: DC – 100 MHz
- Yokogawa 701947 100: 1 Passive Voltage Probe, Bandwidth: DC – 200 MHz
- Yokogawa 701930 Current Probe, Bandwidth: DC – 10 MHz
- AEMC MR561 150/1500 A AC/DC Current Probes, Bandwidth: DC – 10 kHz
- Fluke i400s 400 A AC Current Clamp, Bandwidth: 5–10 kHz.
- LEM LA205-S/SP21 across 50 Ω resistor, Bandwidth: DC – 100 kHz

Scope channel assignments varied depending on the particular test, but in most cases, the signals were measured using the probes and input modules as specified in Table 2. The DL850 was set to 2 MS/s for the line-frequency waveform captures (i.e., FLI and GCI waveforms) and 50 MS/s for the switching-frequency waveform captures (i.e., DAB waveforms).

Table 2. DAQ Signals, Probes, Input Modules, and Bandwidth (BW) Limits

(Pos = Positive, Neu = Neutral, GND = Ground, Pri = Primary, Sec = Secondary)

Input Signal	Probe	Probe BW	Probe Scaling	Probe Measurement Range	Min Value	Max Value	Polarity	Input Module	Input Module Bandwidth	Channel BW Limit
HFX_Vpri	Yokogawa 700929 Isoprobe	DC – 100 MHz	10:1		-600 V	+600 V		720210	20 MHz	Full
HFX_Vsec	Yokogawa 700929 Isoprobe	DC – 100 MHz	10:1		-600 V	+600 V		720210	20 MHz	Full
HFX_Ipri	LEM LA205-S/SP21 across 50Ω resistor	DC – 100 kHz	16.7 mV/A	±500 A	-500 A	+500 A	Pos from Pri to Sec	720210	20 MHz	160 kHz
HFX_Ipri	LEM LA205-S/SP21 across 50Ω resistor	DC – 100 kHz	16.7 mV/A	±500 A	-500 A	+500 A	Pos from Pri to Sec	720210	20 MHz	160 kHz
VDCpri	Yokogawa 700929 Isoprobe	DC – 100 MHz	10:1		0 V	+600 V		701260	40 kHz	Full
VDCsec	Yokogawa 700929 Isoprobe	DC – 100 MHz	10:1		0 V	+600 V		701260	40 kHz	Full
VDCpri-GND	Yokogawa 700929 Isoprobe	DC – 100 MHz	10:1		-600 V	+600 V	Pos on DCPri Pos	720210	20 MHz	Full
VDCsec-GND	Yokogawa 700929 Isoprobe	DC – 100 MHz	10:1		-600 V	+600 V	Pos on DCSec Pos	720210	20 MHz	Full
FLI_Van	Yokogawa 700929 Isoprobe	DC – 100 MHz	10:1		-170 V	+170 V		701260	40 kHz	Full
FLI_Vbn	Yokogawa 700929 Isoprobe	DC – 100 MHz	10:1		-170 V	+170 V		701260	40 kHz	Full
FLI_Vcn	Yokogawa 700929 Isoprobe	DC – 100 MHz	10:1		-170 V	+170 V		701260	40 kHz	Full
TQG_Van	Yokogawa 700929 Isoprobe	DC – 100 MHz	10:1		-170 V	+170 V		701260	40 kHz	Full
TQG_Vbn	Yokogawa 700929 Isoprobe	DC – 100 MHz	10:1		-170 V	+170 V		701260	40 kHz	Full
TQG_Vcn	Yokogawa 700929 Isoprobe	DC – 100 MHz	10:1		-170 V	+170 V		701260	40 kHz	Full
GCI_Vab	Yokogawa 700929 Isoprobe	DC – 100 MHz	10:1		-300 V	+300 V		701260	40 kHz	Full
GCI_Vbc	Yokogawa 700929 Isoprobe	DC – 100 MHz	10:1		-300 V	+300 V		701260	40 kHz	Full
GCI_Vca	Yokogawa 700929 Isoprobe	DC – 100 MHz	10:1		-300 V	+300 V		701260	40 kHz	Full
Grid_Vab	Yokogawa 701947 Isoprobe	DC – 200 MHz	100:1		-300 V	+300 V		701260	40 kHz	Full
Grid_Vbc	Yokogawa 701947 Isoprobe	DC – 200 MHz	100:1		-300 V	+300 V		701260	40 kHz	Full
Grid_Vca	Yokogawa 701947 Isoprobe	DC – 200 MHz	100:1		-300 V	+300 V		701260	40 kHz	Full
VPV2	Yokogawa 701947 Isoprobe	DC – 200 MHz	100:1		0 V	+400 V		701260	40 kHz	Full

VPV3	Yokogawa 701947 Isoprobe	DC – 200 MHz	100:1		0 V	+400 V		701260	40 kHz	Full
VBatt	Yokogawa 700929 Isoprobe	DC – 100 MHz	10:1		0 V	+400 V		701260	40 kHz	Full
In-GND	Yokogawa	DC – 10 MHz	10 mV/A	150 Arms	-200 A	+200 A	Pos from Neu to GND	720210	20 MHz	Full
FLI_Ia	Fluke i400s	5 Hz – 10 kHz	1 mV/A	5 A – 400 A	-200 A	+200 A	Pos out of FLI	701260	40 kHz	Full
FLI_Ib	Fluke i400s	5 Hz – 10 kHz	1 mV/A	5 A – 400 A	-200 A	+200 A	Pos out of FLI	701260	40 kHz	Full
FLI_Ic	Fluke i400s	5 Hz – 10 kHz	1 mV/A	5 A – 400 A	-200 A	+200 A	Pos out of FLI	701260	40 kHz	Full
FLI_In	Hioki CT9693 / CT6590	DC – 15 kHz	1 mV/A	200 Arms	-200 A	+200 A	Pos out of FLI	701260	40 kHz	Full
GCI_Ia	Fluke i400s	5 Hz – 10 kHz	1 mV/A	5 A – 400 A	-200 A	+200 A	Pos into GCI	701260	40 kHz	Full
GCI_Ib	Fluke i400s	5 Hz – 10 kHz	1 mV/A	5 A – 400 A	-200 A	+200 A	Pos into GCI	701260	40 kHz	Full
GCI_Ic	Fluke i400s	5 Hz – 10 kHz	1 mV/A	5 A – 400 A	-200 A	+200 A	Pos into GCI	701260	40 kHz	Full
Load_Ia	Fluke i400s	5 Hz – 10 kHz	1 mV/A	5 A – 400 A	-200 A	+200 A	Pos to Load	701260	40 kHz	Full
Load_Ib	Fluke i400s	5 Hz – 10 kHz	1 mV/A	5 A – 400 A	-200 A	+200 A	Pos to Load	701260	40 kHz	Full
Load_Ic	Fluke i400s	5 Hz – 10 kHz	1 mV/A	5 A – 400 A	-200 A	+200 A	Pos to Load	701260	40 kHz	Full
IPV2	AEMC MR 561	DC – 10 kHz	10 mV/A	150 A	0	20 A	Pos from PV	701260	40 kHz	Full
IPV3	AEMC MR 561	DC – 10 kHz	10 mV/A	150 A	0	20 A	Pos from PV	701260	40 kHz	Full
Ibatt	AEMC MR 561	DC – 10 kHz	10 mV/A	150 A	0	20 A	Pos from Battery	701260	40 kHz	Full

5. Experimental Results

Referring to Table 1, the CUBE-V2 was tested in the following key operating modes:

- Batt Only: FLI regulates main AC bus, BCD regulates DC bus (shaded in pink)
- Grid Only: FLI regulates main AC bus, GCI regulates DC bus (shaded in blue)
- Dsl+Batt+Grid: TQG regulates main AC bus, FLI regulates DC bus, both BCD and GCI in Current Control mode (shaded in yellow)

With the exception of PV-Only mode, the selected operating modes fully exercise the relevant combinations of primary regulating components. For each operating mode, the CUBE was subjected to load or reference steps up and down. Both steady-state and transient waveforms were captured.

5.1. Battery-Only Results

Operation of the CUBE in Battery-Only mode was performed with the battery simulator set to 300 V. In the plots that follow:

- Figure 7 shows the FLI output waveforms when subjected to ± 30 kW balanced load steps.
- Figure 8 shows the DAB HFX waveforms during operation of the FLI at no load and at 30-kW balanced load. These are the voltages and currents measured directly on the primary and secondary sides of the HFX.
- Figure 9 compares the FLI output waveforms at a balanced 21-kW load and at an unbalanced 21-kW load with Ph A = 12 kW, Ph B = 6 kW, and Ph C = 3 kW.
- Figure 10 compares the DAB HFX waveforms during operation of the FLI at a balanced 21-kW load and at an unbalanced 21-kW load with Ph A = 12 kW, Ph B = 6 kW, and Ph C = 3 kW.

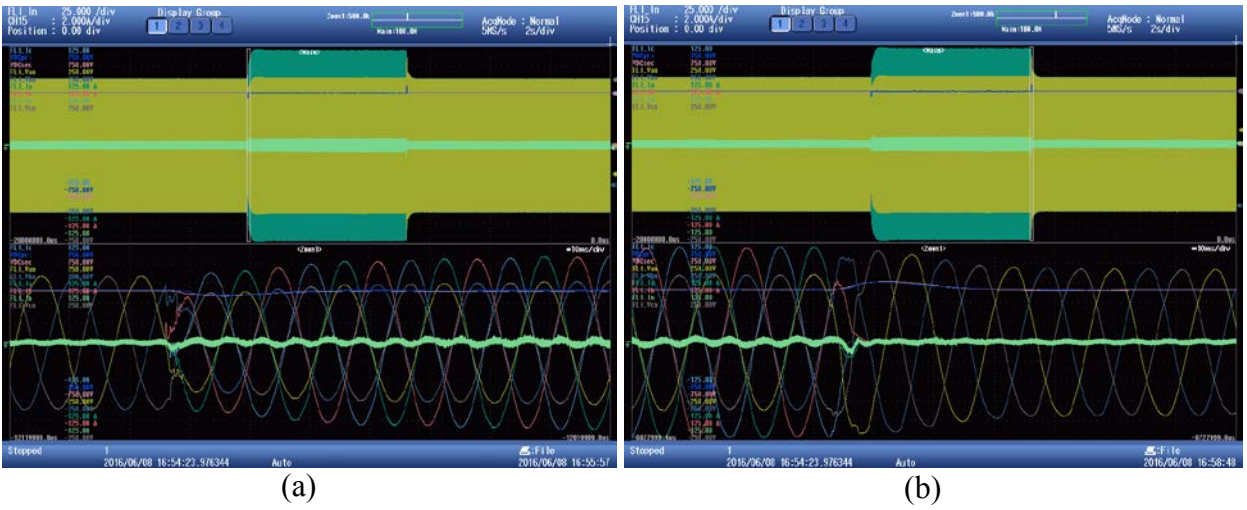


Figure 7. CUBE in Battery-Only mode, FLI waveforms during (a) +30-kW and (b) -30-kW balanced load steps.

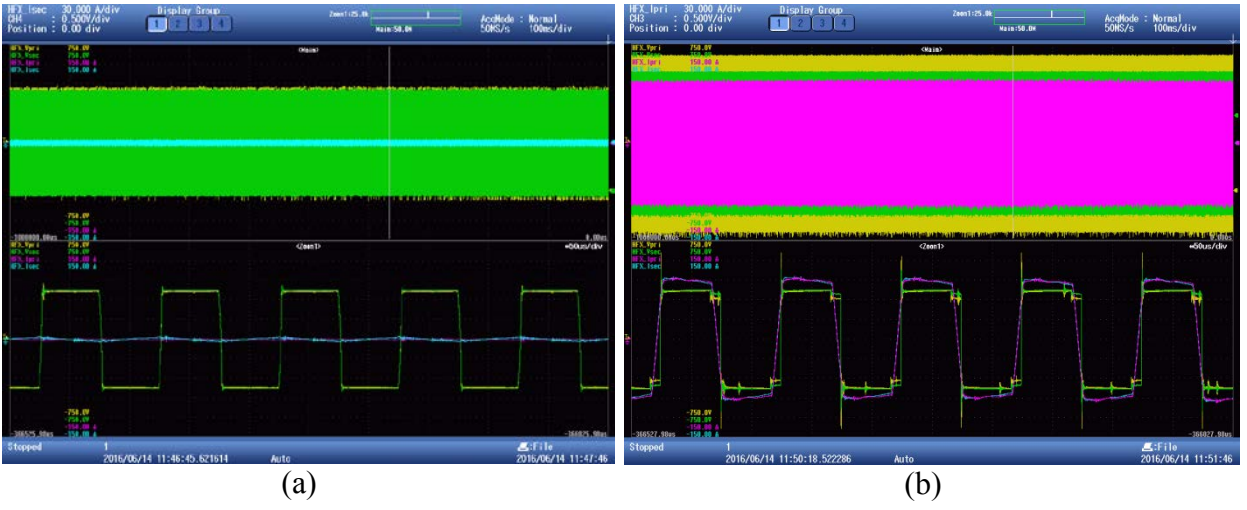


Figure 8. CUBE in Battery-Only mode, HFX waveforms at (a) no load and (b) 30-kW balanced load.

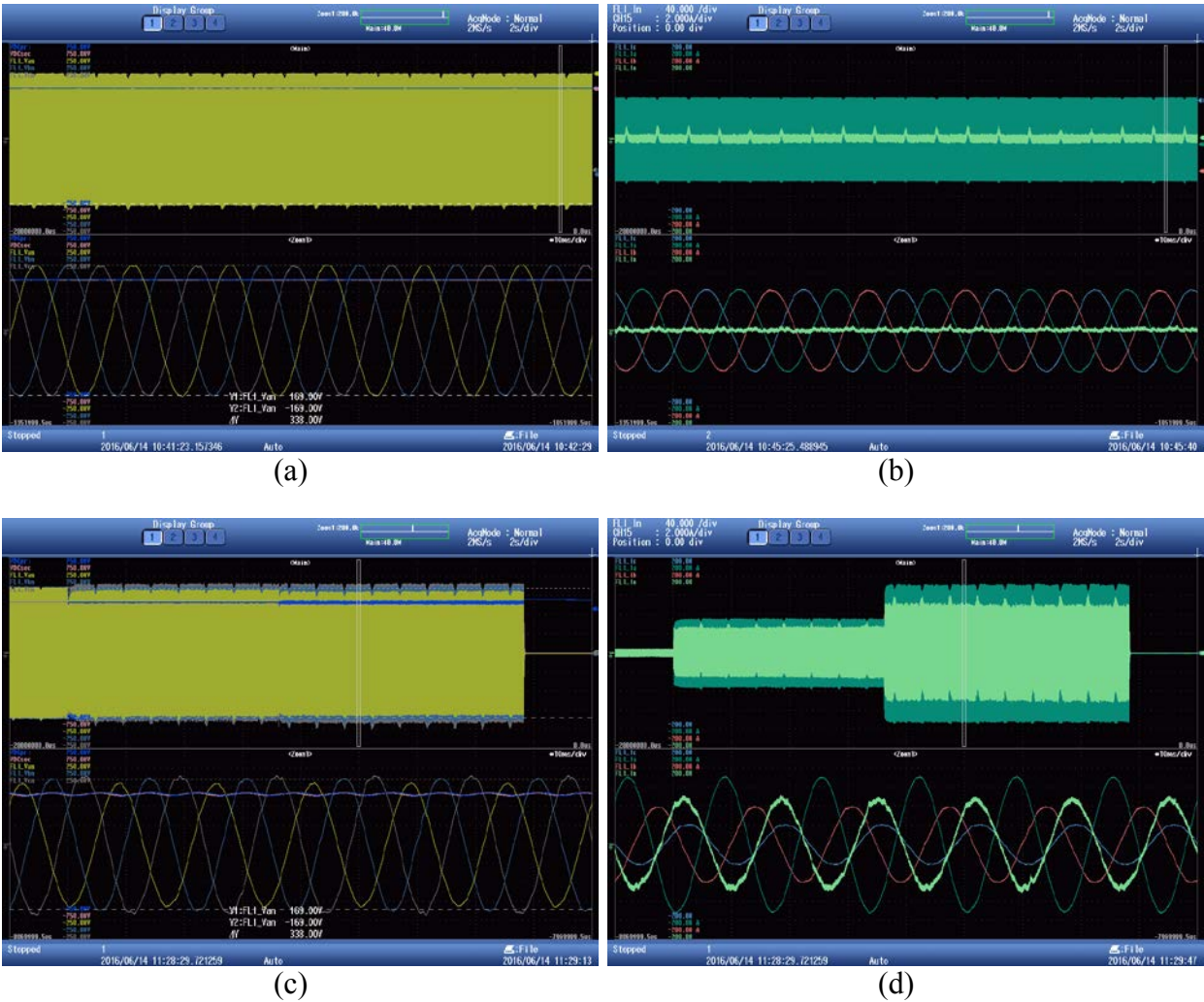


Figure 9. CUBE in Battery-Only mode and high proportional gain for 0-component of FLI voltage control PID feedback loop, FLI voltage and current waveforms at balanced 21-kW load (a,b) and unbalanced (c,d) load with $P_{hA} = 12$ kW, $P_{hB} = 6$ kW, and $P_{hC} = 3$ kW.



Figure 10. CUBE in Battery-Only mode and high proportional gain for 0-component of FLI voltage control PID feedback loop, DAB waveforms at (a) 21-kW balanced load and (b) unbalanced load of PhA = 12 kW, PhB = 6 kW, and PhC = 3 kW.

Observations during Battery-Only Operation

- The FLI is able to deliver sinusoidal output voltage waveform with no visible distortion for balanced loads.
- The FLI transient response to balanced load steps is good although there is $\frac{1}{4}$ -cycle distortion in the AC voltage waveform.
- The FLI is able to maintain reasonable voltage balance in the presence of severe load imbalance. However, it was necessary to substantially increase the FLI voltage control 0-component proportional gain to accomplish this, resulting in slight distortion of the AC voltage waveform and slow 1-Hz oscillations in the neutral current. This may be a simple tuning issue or may be due to coupling of the dq0 feedback loops. This should be explored further.
- The DAB HFX current waveforms are trapezoidal, as expected. The current waveforms do not exhibit any spikes or ringing at switching events; however, these measurements were taken with a sensing bandwidth of 100 kHz. Measurements should be repeated with a higher-bandwidth probe.
- The DAB HFX voltage waveforms exhibit spikes and ringing at switching events. These are due to hard-switching of the leading-edge full bridge and will be discussed further in Section 5.3. The ringing is around 2 MHz (sensing bandwidth is 20 MHz). It is not clear whether this is excitation of parasitics in the actual power circuit or if this is induced in the sensing circuit. Increasing the bandwidth of the current measurements may help answer this question.

5.2. GCI-Only Results

Operation of the CUBE in Grid-Only mode was performed with the grid simulator configured to generate three-phase 120 V_{l-n} (208 V_{l-l}) but 50-Hz instead of 60-Hz voltage. In the plots that follow:

- Figure 11 shows the FLI output waveforms when subjected to ± 15 -kW balanced load steps.
- Figure 12 shows the DAB HFX waveforms during operation of the FLI at no load and at 15-kW balanced load.
- Figure 13 compares the FLI output waveforms at a balanced 15-kW load and at an unbalanced 14-kW load with Ph A = 8 kW, Ph B = 4 kW, and Ph C = 2 kW.
- Figure 14 compares the DAB HFX waveforms during operation of the FLI at a balanced 15-kW load and at an unbalanced 14-kW load with Ph A = 8 kW, Ph B = 4 kW, and Ph C = 2 kW.

The load steps for Grid-Only operation were smaller than those for Battery-Only operation due to the 50-A rating of the grid simulator and requirement for the grid simulator to also supply the magnetizing current to the line-frequency transformer.

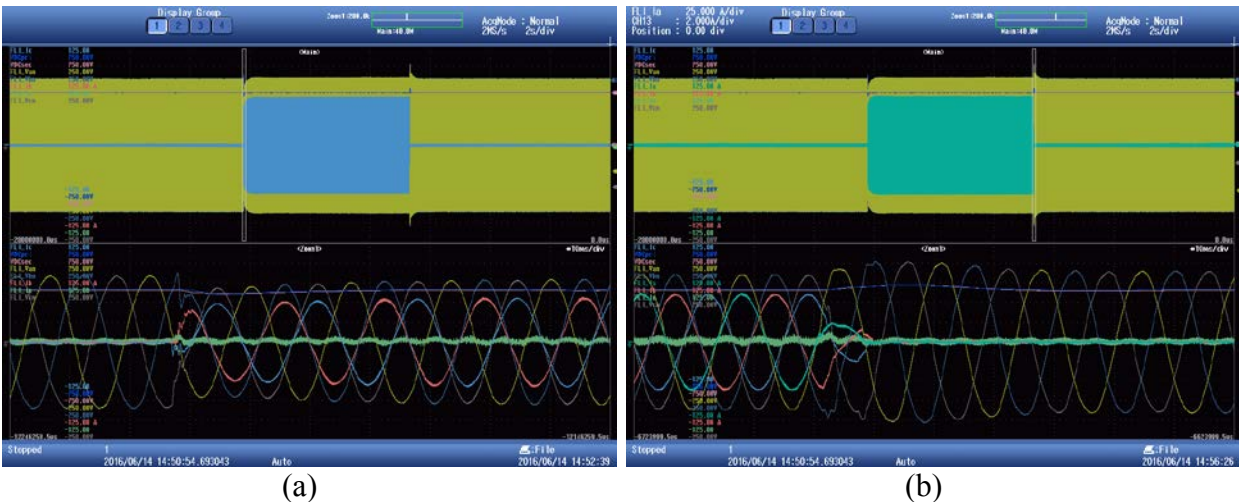


Figure 11. CUBE in Grid-Only mode, FLI waveforms during (a) +15-kW and (b) -15-kW balanced load steps.

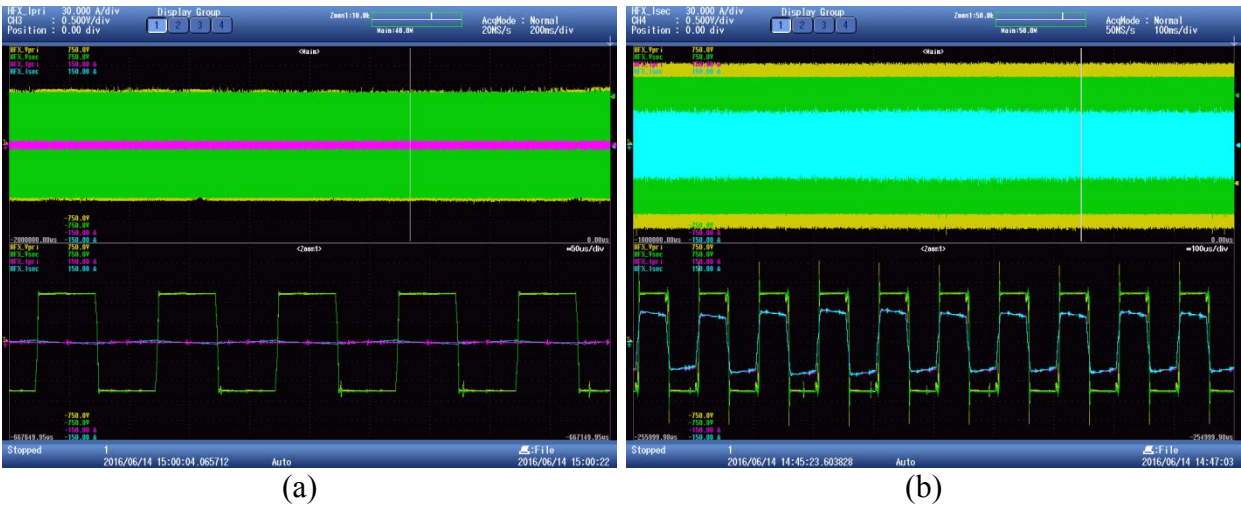
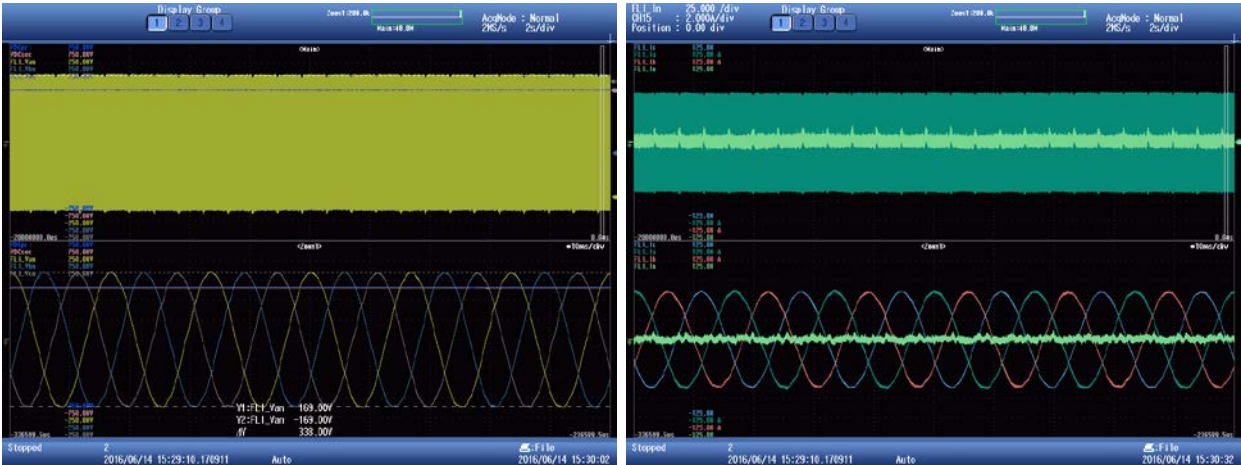
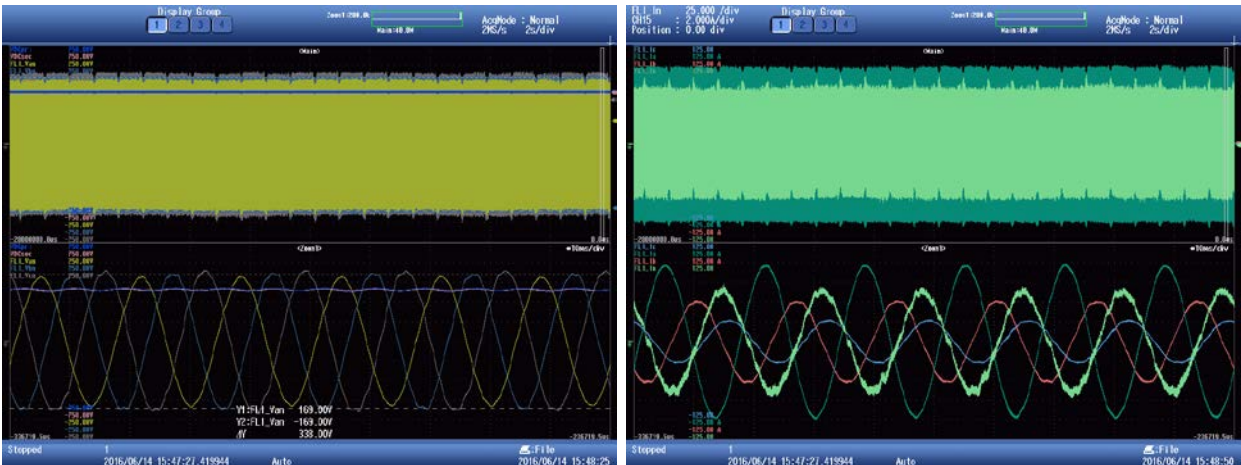


Figure 12. CUBE in Grid-Only mode, DAB waveforms at (a) no load and (b) 15-kW balanced load.



(a)

(b)



(c)

(d)

Figure 13. CUBE in Grid-Only mode and high proportional gain for 0-component of FLI voltage control PID feedback loop, FLI voltage and current waveforms at balanced 15-kW load (a,b) and unbalanced load (c,d) with PhA = 8 kW, PhB = 4 kW, and PhC = 2 kW.

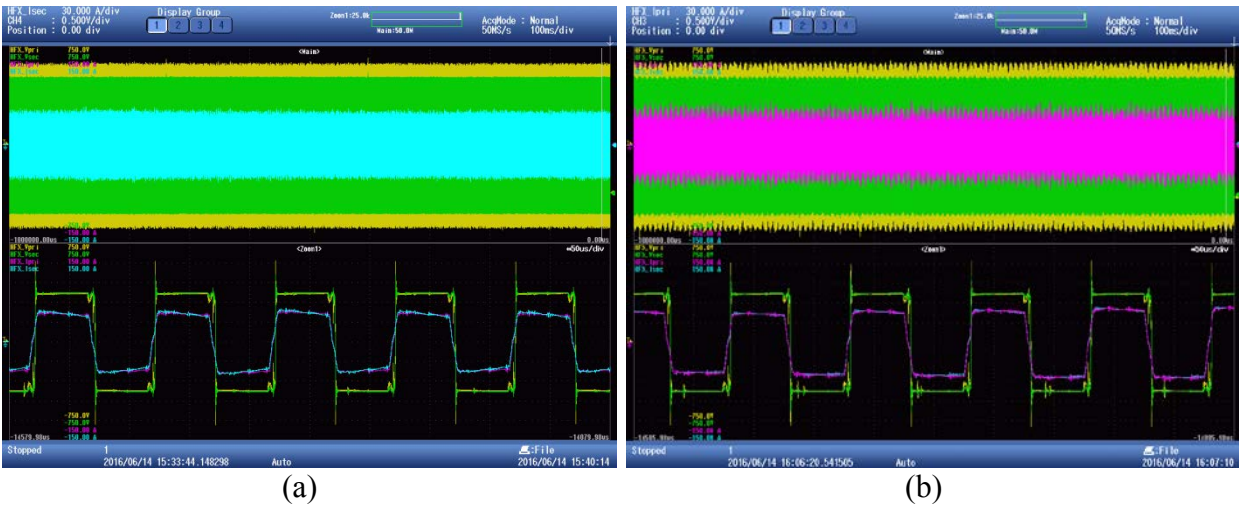


Figure 14. CUBE in Grid-Only mode and high proportional gain for 0-component of FLI voltage control PID feedback loop, DAB waveforms at (a) 15-kW balanced load and (b) unbalanced load of PhA = 8 kW, PhB = 4 kW, and PhC = 2 kW.

Observations during Grid-Only Operation

- Operation during Grid-Only operation is similar to operation during Battery-Only operation.

5.3. Diesel + Battery + Grid Results

Operation of the CUBE in Diesel + Battery + Grid mode was performed with the battery simulator set to 300 V and the grid simulator configured to generate three-phase 100 V_{L-n} (173 V_{L-L}) 50-Hz voltage.

- Figure 15 shows the battery input current and FLI output waveforms during 0 to +67 A and +67 to 0 A steps in battery reference current (grid reference current = 0).
- Figure 16 shows the battery input current and FLI output waveforms during 0 to -67 A and -67 to 0 A steps in battery reference current (grid reference current = 0).
- Figure 17 shows the battery input current and FLI output waveforms during operation at a battery reference current of -67 A, and during a 0 to -50 A step in battery reference current (grid reference current = 0).
- Figure 18 shows the GCI and FLI output waveforms during 0 to -50 A and -50 to 0 A steps in grid reference current (battery reference current = 0).
- Figure 19 shows the GCI and FLI output waveforms during 0 to -50 A and -50 to 0 A steps in grid reference current (battery reference current = 0).
- Figure 20 shows the DAB HFX waveforms during operation at battery reference currents of +67 A and -67 A (grid reference current = 0).
- Figure 21 shows 10 μ s/div zooms of the DAB HFX waveforms during operation at battery reference currents of +67 A and -67 A (grid reference current = 0).

The 50-A grid-current reference steps are equivalent to 15 kW and were limited by the current rating of the grid simulator.

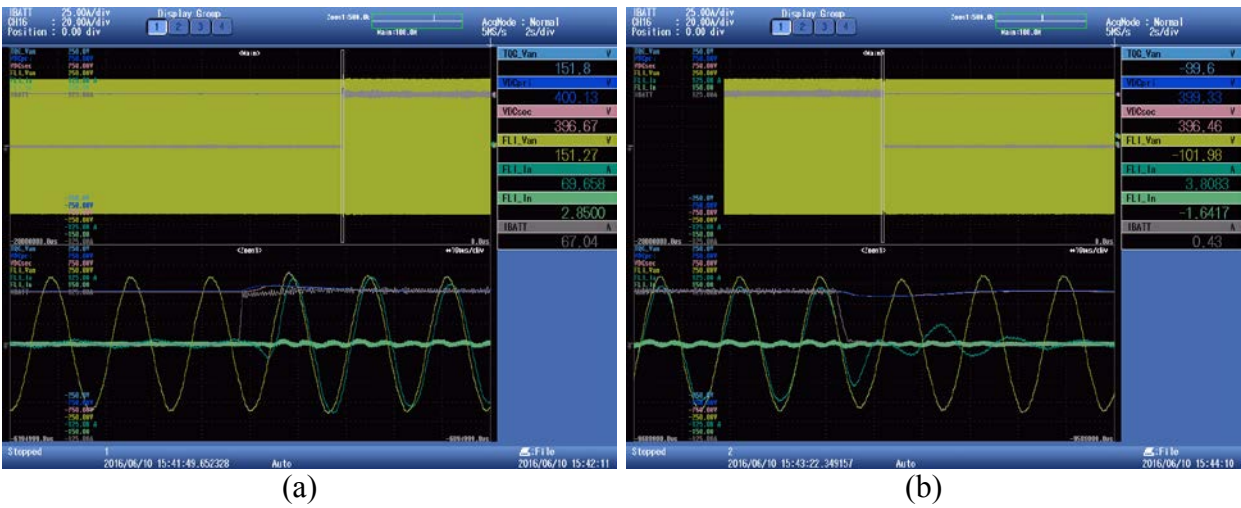


Figure 15. CUBE in Diesel + Battery + Grid mode and 25-kW load applied, FLI and BCD waveforms during (a) 0 to +67 A and (b) +67 to 0 A steps in battery reference current, with grid reference current = 0.

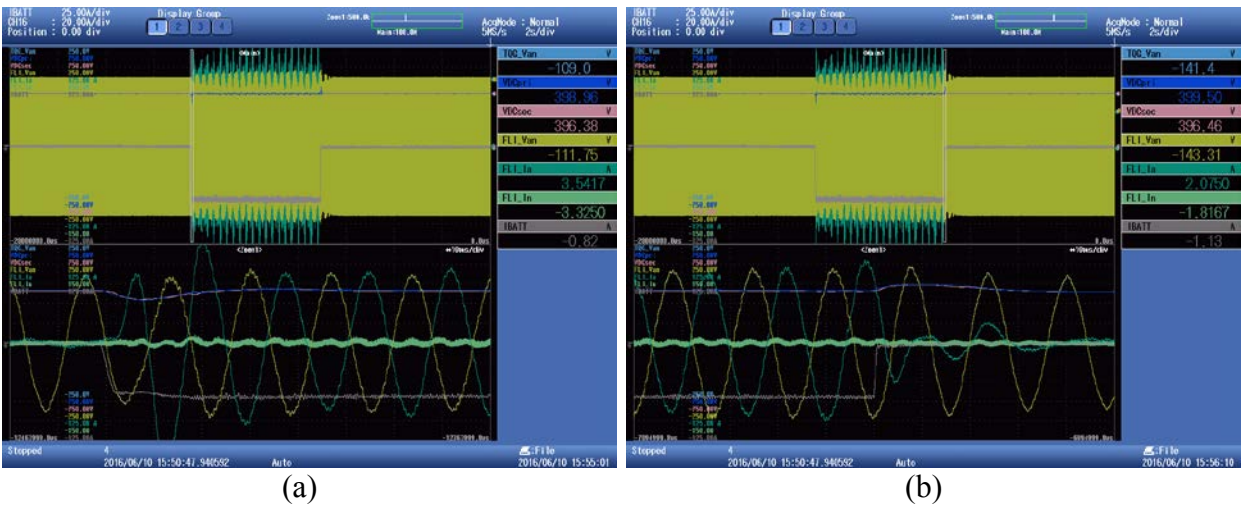


Figure 16. CUBE in Diesel + Battery + Grid mode and no load, FLI and BCD waveforms during (a) 0 to -67 A and (b) -67 to 0 A steps in battery reference current, with grid reference current = 0.

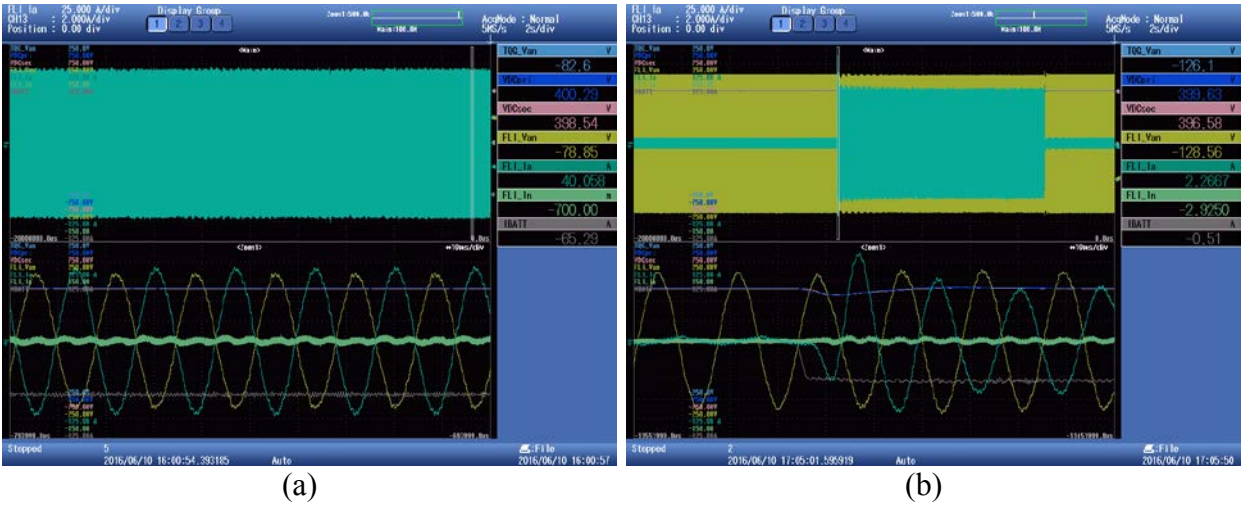


Figure 17. CUBE in Diesel + Battery + Grid mode and no load, FLI and BCD waveforms during (a) - 67 A steady state and (b) 0 to -50 A steps in battery reference current, with grid reference current = 0.

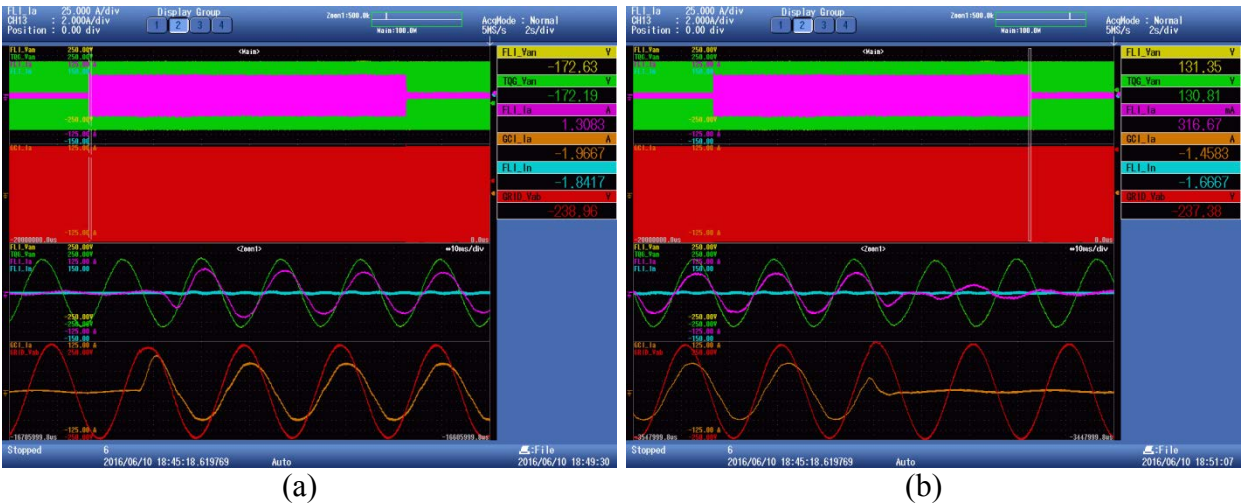


Figure 18. CUBE in Diesel + Battery + Grid mode and 25-kW load applied, FLI and GCI waveforms during (a) 0 to -50 A and (b) -50 to 0 A steps in grid reference current, with battery reference current = 0.

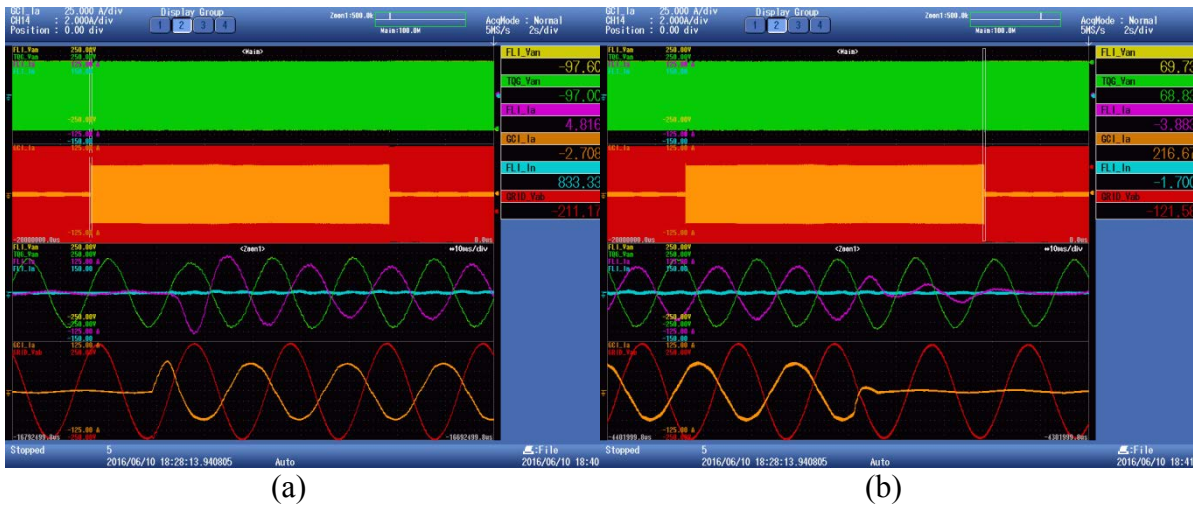


Figure 19. CUBE in Diesel + Battery + Grid mode and no load, FLI and GCI waveforms during (a) 0 to +50 A and (b) +50 to 0 A steps in grid reference current.

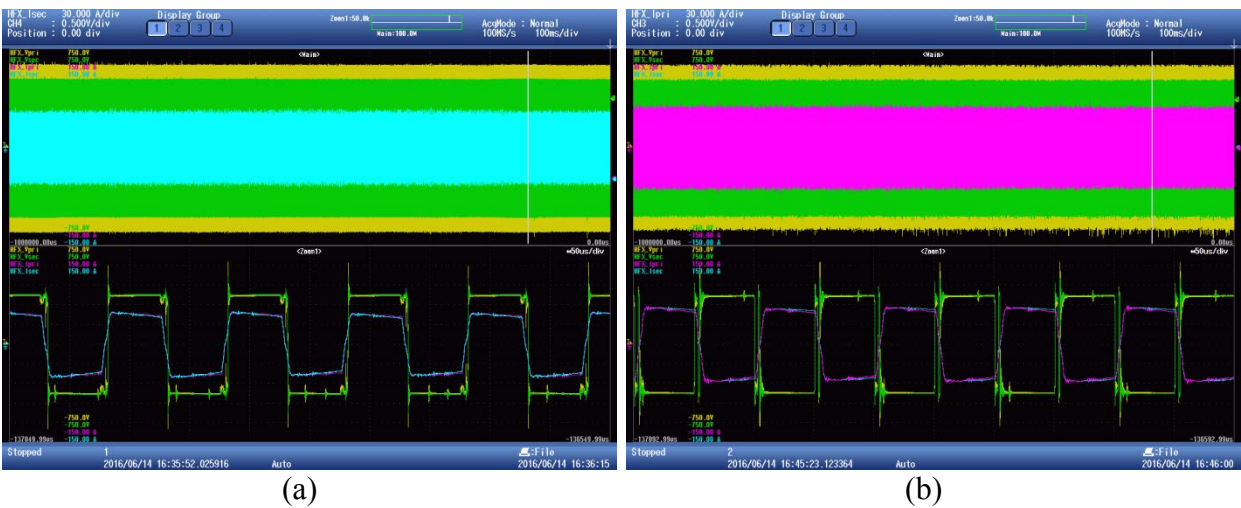


Figure 20. CUBE in Diesel + Battery + Grid mode, DAB waveforms at (a) 25-kW load and battery reference current of +67 A and (b) no load and battery reference current of -67 A, with grid reference current = 0.

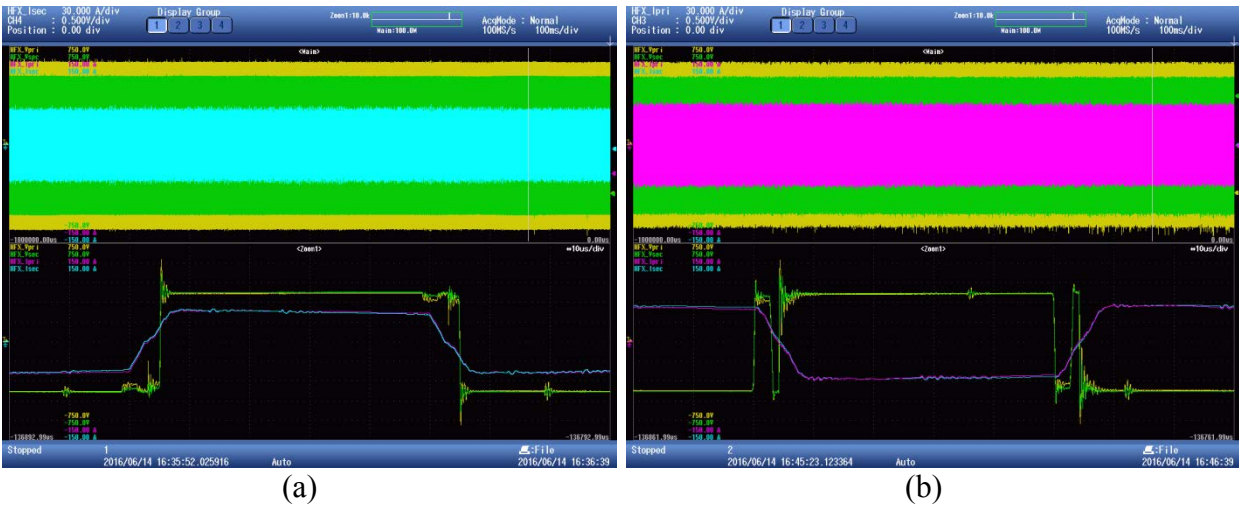


Figure 21. CUBE in Diesel + Battery + Grid mode, 10 μ s/div zooms of DAB waveforms at (a) 25-kW load and battery reference current of +67 A and (b) no load and battery reference current of -67 A, with grid reference current = 0.

Observations during Operation with Diesels, Battery, and Grid

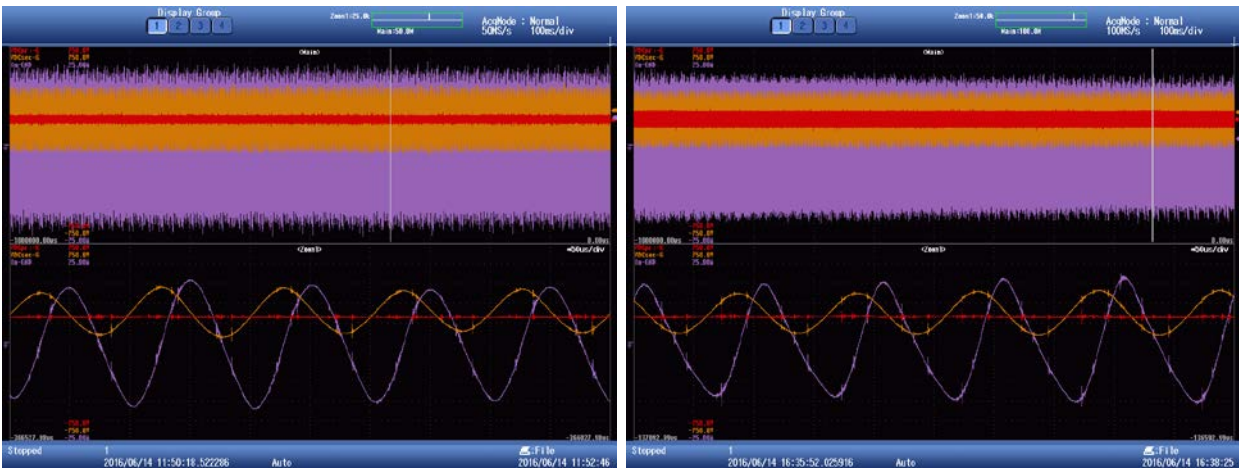
- The FLI is able to source sinusoidal current with no visible distortion at balanced loads. However, there is harmonic distortion at about 1.6 kHz when the FLI is sinking large currents. This is worse for operation with the battery than for operation with the grid with the harmonic oscillations barely visible when supplying 50 A back to the grid, but clearly visible when charging the battery at 50 A. This should be explored further and may require addition of damping filters in the circuit(s).
- The transient response to all reference steps is excellent with the exception of the response to large negative battery reference current steps that can introduce persistent slow oscillations. This is apparent in the 3.7-Hz oscillations triggered by the -67 A reference step in Figure 16. These are not triggered when the reference is ramped to -67 A in at least two steps, which was the case for the waveforms shown in Figure 17. It is possible that this is partially an aliasing problem that could be addressed by decreasing the corner frequency of the FLI current-sensing input filter. It is also possible that this is a stability issue that may also benefit from adding damping filters to the circuit(s). This should also be explored further.
- The 10 μ s/div zooms of the DAB HFX waveforms in Figure 21 are illuminating. They indicate loss of ZVS (hard-switching) for the leading-side full bridge. The leading-side full bridge is the one that switches polarity first. In the leading-side full-bridge, the IGBTs primarily (i.e., outside of switching transitions) conduct, while in the lagging-side full-bridge, the anti-parallel diodes primarily conduct. During operation at positive battery current (herein referred to as “forward power flow”), the primary-side full bridge is the leading-side. During operation at negative battery current (herein referred to as “reverse power flow”), the secondary-side full bridge is the leading-side. The loss of ZVS during the leading-side full-bridge transition can be explained as follows:

When the currently conducting diagonal set of IGBTs on the leading-side full bridge are gated off, the inductor current forward-biases the anti-parallel diodes associated with the opposing diagonal set of IGBTs, causing the voltage across that full bridge to change polarity and the inductor current to ramp towards zero. ZVS would be achieved if those IGBTs could be gated on while their anti-parallel diodes were still conducting. However, due to the interlock dead time between gating of the top and bottom SKAI IGBTs within each half-bridge, the inductor current reaches zero before these IGBTs are gated on. When the inductor current reaches zero, the diodes turn off and the voltage across the leading-side full-bridge becomes that imposed by the lagging-side full-bridge (since inductor current equals zero). Because the lagging-side full-bridge has not yet switched state, that voltage is of the original polarity and the voltage across the leading-side full-bridge also changes back to the original polarity, and the inductor current remains at zero. After the dead time has elapsed, the IGBTs turn on and cause the voltage across the leading-side full-bridge to change once more and the inductor current to resume its ramp. This transition does not occur at ZVS as desired. The subsequent lagging-side transition does occur at ZVS because the transition ends the inductor ramp rather than initiates it; therefore, current does not ramp to zero and the conducting diodes remain forward biased no matter how long the dead time. The loss of ZVS is most clearly seen in the reverse power operation of Figure 21(b) due to the fact that the measured HFX voltage directly reflects the voltage across the secondary-side full bridge, whereas the voltage across the primary-side full bridge is decoupled from the HFX voltage by the resonant inductor. However, it is still present during forward power operation, and it occurs regardless of CUBE operating mode.

For this design, the loss of ZVS is caused by dead times that are long relative to the switching frequency. In particular, the SKAIs used to build the CUBE are 2012 beta versions with a dead time of 4.5 μs , whereas they are being driven at 10 kHz (100 μs). The resulting hard-switching contributes to higher than expected losses. Although the losses in this case are restricted to losses associated with stored energy in the IGBT output capacitances, rather than the much larger losses associated with diode reverse recovery; this issue needs to be addressed.

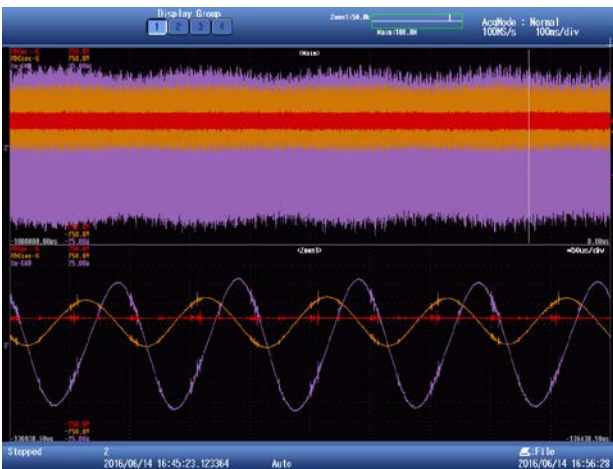
5.4. Leakage Current

The SKAI modules include electromagnetic interference (EMI) filtering capacitors from each of the positive and negative DC terminals to chassis (Y-caps). Direct connection of the ground-referenced main AC bus to the FLI creates a common-mode circuit between the main AC bus and the secondary-side DC bus through the Y-caps. This circuit is excited by the high-frequency common-mode voltage imposed onto the secondary-side DC bus from the FLI modulation, resulting in high-frequency leakage current. Figure 22 shows the secondary-side DC bus common-mode voltage (positive terminal with respect to ground) and the leakage current measured on the bonding jumper between the main A bus neutral and ground. Typical RMS values are 225 V and 8 A, respectively. This will be addressed by investigating alternate four-leg inverter modulation strategies with reduced high-frequency common-mode components and/or by adding a common-mode inductor on the FLI output.



(a)

(b)



(c)

Figure 22. Leakage current and common-mode voltage on the secondary-side DC bus during operation (a) in Battery-Only mode at 30 kW, and (b) Diesel + Battery + Grid mode, 25-kW load, battery reference current = +67 A, and (c) Diesel + Battery + Grid mode, 5-kW load, battery reference current = -67 A.

5.5. Efficiency

Observations based on power as displayed on the CUBE user interface during Diesel + Battery operation indicate an end-to-end efficiency between the battery terminals and the FLI terminals (i.e., including the BCD, DCX, and FLI) of 90%–91% when discharging the battery at 20 kW and 88%–89% when charging the battery at 20 kW. However, further work would be required to properly instrument the CUBE for more reliable efficiency calculations.

6. Conclusions and Future Work

In this project, several modifications and improvements to the CUBE-V1 design were implemented and validated at NREL. These improvements included a decrease in the total size and weight of the design, ability to balance voltage under unbalanced load conditions, and provision for a connection to a host utility with varying frequency, voltage, and power quality.

To validate the design modifications, experimental waveforms were captured during operational testing of the CUBE-V2 to verify new functionalities as well as observe output power quality and dynamic response. As shown in this report, the experimental results indicate that the intended design targets were achieved.

Specifically, combined operation of a dual-active bridge (DAB) and a four-leg inverter (FLI) can provide the galvanic isolation and neutral connection traditionally supplied by a three-leg inverter and line-frequency transformer with significantly reduced weight and volume (a 55% reduction in volume and a 70% reduction in weight relative to the line-frequency transformer). Furthermore, the DAB-FLI solution can provide voltage-balancing functionality that the traditional configuration could not. Provision for connection to a host utility through the improved design was also validated.

The advantages demonstrated by the CUBE-V2 design are significant improvements upon the CUBE-V1 design, making it lighter, smaller, and more flexible for field operations. These improvements should yield logistical and operational benefits to mobile electric power systems such as those employed to provide power to Forward Operating Bases and Command Outposts.

Future work includes resolving the following outstanding issues: (1) mitigation of leakage current, ideally by investigating FLI modulation algorithms with reduced high-frequency common-mode components; (2) investigation of the cause of and means to mitigate harmonics present when the FLI is supplying power back to the DC bus; (3) tuning of system dynamics and/or decoupling of dq0 feedback loops to achieve the ability to balance system voltages in the presence of severe load imbalance without introducing voltage distortion or oscillations in neutral current; and (4) investigation of methods to maintain ZVS despite relatively long IGBT dead times. In addition to these issues, the end-to-end efficiency of the CUBE during each of the operating modes should be properly characterized.

7. References

1. DeDoncker, R.W.; Divan, D.M.; and Kheraluwala, M.H. "A Three-Phase Soft-Switched High-Power-Density dc/dc Converter for High-Power Applications." *IEEE Transactions on Industry Applications* (27:1), Jan/Feb 1991, pp. 63–73.
2. DeDoncker, R.W.; Divan, D.M.; and Kheraluwala, M.H. U.S. Patent No. 5,027,264, Jun. 25, 1991.
3. Zhao, B.; Song, Q.; Whenua, L.; and Sun, Y. "Overview of Dual-Active-Bridge Isolated Bidirectional DC-DC Converter for High-Frequency-Link Power-Conversion System." *IEEE Transactions on Power Electronics* (29:8), Aug. 2014, pp. 4091–4106.
4. Oriz, G.; Uemura, H.; Bortis, D.; and Kolar, J.W. "Modeling of Soft-Switching Losses of IGBTs in High-Power High-Efficiency Dual-Active-Bridge DC/DC Converters." *IEEE Transactions on Electronic Devices* (60:2), Feb. 2013, pp. 587–597.
5. Krismer, F.; Biela, J.; and Kolar, J.W. "A Comparative Evaluation of Isolated Bi-directional DC/DC Converters with Wide Input and Output Voltage Range." *Conference Record of the 2005 Industry Applications Society Meeting, Vol. 1*; Oct. 2–6, 2005, Hong Kong, China; pp. 599–606.
6. Karshenas, H.R.; Daneshpajoo, H.; Safaee, A.; Jain, P.; and Bakhshai, A. "Bidirectional DC-DC Converters for Energy Storage Systems," Chapter 8. Carbone, R., ed. *Energy Storage in the Emerging Era of Smart Grids*. InTech, 2011; pp. 161–178.
<http://www.intechopen.com/books/energy-storage-in-the-emerging-era-of-smart-grids>
7. Krismer, F. *Modeling and Optimization of Bidirectional Dual Active Bridge DC-DC Converter Topologies*. Ph.D. Thesis. Zurich, Switzerland: ETH Zurich, 2010.
8. Kheraluwala, M.H., Gascoigne, R.W., Divan, D.M., and Baumann, E.D. "Performance Characterization of a High-Power Dual Active Bridge dc-to-dc Converter," *IEEE Transactions on Industry Applications*, (28:6), pp. 1294–1301, Nov/Dec 1992.
9. Schibli, N. *Symmetrical Multilevel Converters with Two Quadrant DC-DC Feeding*. Ph.D. Thesis. Lausanne, Switzerland. Swiss Federal Institute of Technology Lausanne (EPFL), 2000.
10. Bai, H., and Mi, C., "Eliminate Reactive Power and Increase System Efficiency of Isolated Bidirectional Dual-Active-Bridge DC-DC Converters Using Novel Dual-Phase-Shift Control," *IEEE Transactions on Power Electronics* (23:6), Nov. 2008, pp. 2905–2914.
11. Oggier, C.G., Garcia, G.O., and Oliva, A.R., "Switching Control Strategy to Minimize Dual Active Bridge Converter Losses," *IEEE Transactions on Power Electronics* (24:7), July 2009, pp. 1826–1838.
12. Zhang, R. *High Performance Power Converter Systems for Nonlinear and Unbalanced Load/Source*. Ph.D. Thesis. Blacksburg, VA: Virginia Polytechnic Institute and State University, 1998.
13. Zhang, R., Prasad, V.H., Boroyevich, D., and Lee, F.C., "Three-Dimensional Space Vector Modulation for Four-Leg Voltage-Source Converters," *IEEE Transactions on Power Electronics* (17:3), May 2002, pp. 314–326.